Earth and Planetary Science Letters 615 (2023) 118214

Contents lists available at ScienceDirect

Earth and Planetary Science Letters

journal homepage: www.elsevier.com/locate/epsl

Titanium isotope evidence for the high topography of Nuna and Gondwana - Implications for Earth's redox and biological evolution

Nikitha S. Saji [a,*,1], Roberta L. Rudnick [b], Richard M. Gaschnig [c], Marc-Alban Millet [a]

[a] School of Earth and Environmental Sciences, Cardiff University, Cardiff CF10 3AT, UK
[b] Department of Earth Science and Earth Research Institute, University of California, Santa Barbara, CA 93106, USA
[c] Department of Environmental, Earth and Atmospheric Sciences, University of Massachusetts Lowell, Lowell, MA 01854, USA

ARTICLE INFO

Article history:
Received 4 November 2022
Received in revised form 4 May 2023
Accepted 6 May 2023
Available online 24 May 2023
Editor: B. Wing

Keywords:
titanium isotopes
supercontinents
eukaryote evolution
oxygenation

ABSTRACT

Titanium isotopes recorded in glacial diamictites with depositional ages between 2.9 and 0.3 Ga show that the upper continental crust became significantly more felsic relative to the present-day crust during the amalgamation of the Paleoproterozoic Nuna and the Neoproterozoic Gondwana supercontinents. This can be attributed to the continental collisions involved in the assembly of Nuna and Gondwana. The resulting high topographic relief of Nuna and Gondwana orogens must have resulted in an enhanced erosional supply from the continents to oceans. The step changes in the development of organismal complexity from prokaryotes to eukaryotes, and eventually metazoans, appear to be temporally correlated to instances where collisional mountain-building sustained an elevated nutrient supply from the continents to oceans. The nutrient surge associated with the rise of the Gondwana mountains likely provided the necessary impetus for the Neoproterozoic ecological expansion of eukaryotes and the eventual radiation of metazoans. A similar link between the enhanced nutrient supply from Nuna mountains and the radiation of early eukaryotes is plausible, although its mechanistic underpinnings remain unclear. The termination of Nuna orogeny and its transition to Rodinia without significant breakup and subsequent collisional orogenesis corresponds to the long lull in Earth's redox and biological evolution in its middle age.

1. Introduction

Surface oxygenation has historically attracted much attention as the trigger for biological complexity with oxygen production considered a prerequisite for the appearance and diversification of metazoans (Nursall, 1959). An important variable that has remained underexplored with respect to the evolution of complex animal life is the role of plate tectonics in modulating the marine nutrient inventory and associated redox changes. It is widely accepted that the long-term source of atmospheric oxygen is primary production and subsequent organic carbon burial in deep-sea sediments, which is ultimately limited by the supply of nutrients from continents to oceans via erosion and weathering (Marais et al., 1992). Over geological timescales, continental weathering rates vary as a function of the composition and elevation of the continental crust and can be linked via feedback mechanisms to the CO_2 concentrations in the atmosphere (Walker et al., 1981). However, weathering rate is ultimately limited by the supply of fresh rock to the surface, which remains a function of erosion rate and denudation (Lenardic et al., 2016). By their very nature, continental arcs develop at convergent plate boundaries where significant tectonic compression and crustal thickening occur, leading to mountain building (Dewey and Bird, 1970). The high topographic relief of orogenic mountain belts, as in the present-day Himalayas, is known to typically increase erosion rates (Galy and France-Lanord, 2001) and possibly exert a significant control on the nutrient supply from continents to oceans (Campbell and Allen, 2008; Tang et al., 2021; Zhu et al., 2022).

Tracking the topographic relief of global continental crust through time, in order to explore its effects on the nutrient availability in oceans, is non-trivial due to the fragmentary nature of the preserved rock record. The chemistry of terrigenous sediments can provide a useful crustal topography record of the past, given that the thicker crust formed in continental arcs and collisional zones of high relief tends to be more differentiated (i.e., more felsic) than the thinner crust formed in oceanic island arcs (Ducea et al., 2015). This is because crustal thickening during mountain

* Corresponding author.
E-mail address: nsaji@centralstate.edu (N.S. Saji).
[1] Present address: College of Engineering, Science, Technology and Agriculture, Central State University, Wilberforce, OH 45384, USA.

https://doi.org/10.1016/j.epsl.2023.118214

building triggers extensive partial melting and granitoid magmatism, resulting in an upper continental crust that, on average, has a highly felsic chemical composition (Hopkinson et al., 2017; Searle, 2013). Episodes of collisional mountain building that likely resulted in enhanced nutrient delivery to the oceans could thus be reflected in the sedimentary record as intervals where felsic lithologies were more abundantly available for erosion. This approach is similar to that adopted by Tang et al. (2021) and Zhu et al. (2022), who respectively used europium (Eu) and lutetium (Lu) abundances in zircon as a proxy for the thickness of active continental crust. The pressure-sensitive nature of Eu and Lu partitioning into zircon during magmatic differentiation can be expected to be coincident with the trend towards increased felsic magmatism as the crust thickens in collisional zones.

Titanium isotopes have recently emerged as a possible proxy for the lithological composition of the upper continental crust (Greber et al., 2017). Significant mass-dependent Ti isotope fractionation occurs during magmatic differentiation in igneous systems with $\delta^{49/47}$Ti values (i.e., per mil deviations relative to the OL-Ti standard; Millet and Dauphas, 2014) progressively increasing from mafic to felsic melt compositions (Millet et al., 2016; Greber et al., 2017; Deng et al., 2019). Fractional crystallization of isotopically light Fe-Ti oxides has been shown to be the dominant mechanism driving the increase in $\delta^{49/47}$Ti values with increasing silica content (Greber et al., 2021; Hoare et al., 2020; Johnson et al., 2019). The $\delta^{49/47}$Ti values measured in terrigenous sediments can therefore be used to infer the upper continental crust lithological composition, which in turn is a measure of crustal elevation to first order. The robustness of this method depends upon the choice of appropriate proxy ratios that can, together with $\delta^{49/47}$Ti, distinguish between the different lithological endmembers, as well as on whether these calculations take into account the secular variations in endmember compositions (Greber and Dauphas, 2019; Keller and Harrison, 2020; Ptáček et al., 2020). In addition, the magnitude of Ti isotope fractionation varies considerably between geodynamic settings depending on redox conditions and initial melt chemistry (Hoare et al., 2020). This leaves Ti isotopes in terrigenous sediments a non-unique indicator of crustal composition unless the secular variation in geodynamic settings that contributed to the generation of continental crust is considered. We circumvent this complication by looking at Ti isotope signatures in the context of immobile element geochemistry that can constrain the sediment provenance characteristics. In this study, we investigate the Ti isotope signatures preserved in glacial diamictites deposited between ~2.9 to 0.3 Ga (Gaschnig et al., 2016) to reconstruct the lithological composition of the global upper continental crust through time. Our results add to a growing body of evidence that suggests that the tempo of collisional mountain building modulated the nutrient supply from continents to oceans through time with important possible implications for the course of Earth's oxygenation history as well as the timing of major advances in biological and ecosystem complexity (Tang et al., 2021; Zhu et al., 2022).

2. Materials and methods

The samples investigated here comprise 24 glacial diamictite composites generated by mixing equal weights of whole rock powders made from the fine-grained matrix of diamictites collected from multiple outcrops for a given formation. These samples have been well characterized for their mineralogy, major and trace element, and a wide variety of isotope compositions. Details of geological context and sample preparation can be found in Gaschnig et al. (2014) and Gaschnig et al. (2016) respectively. The samples investigated here have depositional ages that span the Archean-Proterozoic boundary (~2.9–2.2 Ga) and the Proterozoic-Phanerozoic boundary (~0.7–0.3 Ga) (Supplementary Data Table S1).

Mass-dependent Ti isotope compositions were analyzed following the double spike (DS) protocol of Millet and Dauphas (2014). Approximately 15 - 50 mg of rock powders were digested in 1:1 concentrated HF-HNO_3 mixture at 120°C for ~48 hours. After evaporation to incipient dryness, samples were dissolved in concentrated nitric acid at least three times and finally taken up in 6M HCl and carefully checked for residual solids. If sample solutions were clear, approximately 30 mg of H_3BO_3 was added to the solution to ensure complete dissolution of any remaining fluorides. An aliquot corresponding to 5 - 20 µg of Ti was spiked with a ^{47}Ti - ^{49}Ti double spike in ideal proportions according to the known Ti concentrations for the samples. The sample-DS mixture was dried down and cycled twice through concentrated nitric acid evaporation before being taken up in 12M HNO_3 for chromatographic purification. Ti was purified from the sample matrix using TODGA resin following the procedure of Zhang et al. (2011). The 2 ml TODGA resin cartridges were cleaned and preconditioned with 3M HNO_3 and 12M HNO_3 respectively. The matrix was eluted with 10 ml of 12M HNO_3 and Ti was collected using 10 ml 12M HNO_3-1 wt.% H_2O_2 mixture. The Mo/Ti ratios in the samples are too low (< 0.001%) to affect the accuracy of Ti isotope measurements and therefore further purification using AG1-X8 aimed at Mo removal was not performed.

Ti isotopes were measured in the Nu Plasma II MC-ICP-MS at Cardiff University in high-resolution mode. Samples were dissolved in 0.3 M HNO_3-0.005% HF and aspirated using an Aridus II desolvating nebulizer. All sample measurements were bracketed by measurements of the double-spiked OL-Ti standard (Millet and Dauphas, 2014) at the same concentration and sample-to-spike ratio as the samples. Data reduction was done offline using the in-house double spike convolution code written in ©Mathematica. Ti isotope compositions are reported as $\delta^{49/47}$Ti, representing per mil deviations of the sample ^{49}Ti/^{47}Ti ratio relative to that of OL-Ti standard. The typical uncertainties on $\delta^{49/47}$Ti values are 0.02 to 0.03‰ at 95% confidence. Sample repeats involving separate digestions agreed with each other within error (Supplementary Data Table S1). The rock standard BCR-2 analyzed the same way as the samples returned a $\delta^{49/47}$Ti value indistinguishable from published values, confirming the accuracy of the Ti isotope measurements reported in this study.

3. Results and discussion

3.1. Ti isotopes in diamictites and shales

Globally distributed glacial diamictites with Mesoarchean to Paleozoic depositional ages analyzed in this study have $\delta^{49/47}$Ti compositions that range from 0.13 (±0.04) to 0.38 (±0.03) ‰ (Supplementary Data Table S1). There is considerable scatter in the $\delta^{49/47}$Ti compositions of diamictites with similar depositional ages, and this likely reflects localized provenance effects (Fig. 1). The Mesoarchean and Paleoproterozoic diamictites show relatively limited variability in $\delta^{49/47}$Ti with a mean value of 0.20 ± 0.03 (n=4; 95% c.i.) ‰ and 0.22 ± 0.01 (n=7; 95% c.i.) ‰ respectively. The Neoproterozoic diamictites, on the other hand, show larger variability in their $\delta^{49/47}$Ti values with a resolvably higher mean $\delta^{49/47}$Ti of 0.32 ± 0.01 (n=10; 95% c.i.) ‰. There is a statistically significant difference in $\delta^{49/47}$Ti between the Paleoproterozoic and Neoproterozoic diamictite means ($p < 0.01$). Our new glacial diamictite data contrast with the earlier results of Greber et al. (2017) who investigated the $\delta^{49/47}$Ti values of shales, and suggested that the global upper continental crust had a relatively uniform and invariant Ti isotope composition since ~3.5 Ga. By contrast, our data show resolvable variations towards higher $\delta^{49/47}$Ti

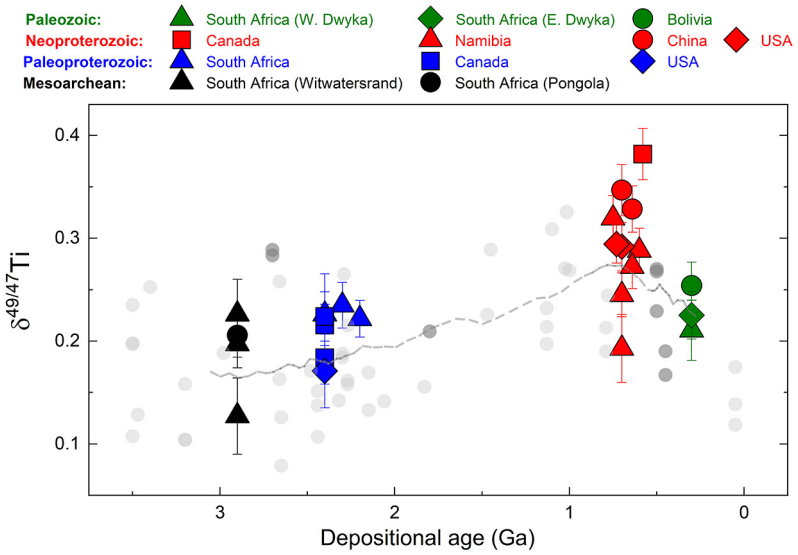

Fig. 1. The $\delta^{49/47}$Ti values of glacial diamictites analyzed in this study plotted as a function of their depositional ages from Gaschnig et al. (2016). Error bars represent 95% confidence intervals. Also shown in grey circles are the $\delta^{49/47}$Ti values of individual shales from Greber et al. (2017) (light-shaded) and Deng et al. (2019) (dark-shaded). The dashed line represents a moving average of the individual shale and diamictite data pooled together.

in the Neoproterozoic diamictites relative to the contemporaneous shale average. The average $\delta^{49/47}$Ti values of Mesoarchean, Paleoproterozoic, and Paleozoic diamictites are, nevertheless, indistinguishable from that of the contemporaneous shales from Greber et al. (2017). On closer inspection, it is evident that the individual shale data from Greber et al. (2017) follow a somewhat similar temporal pattern as the glacial diamictites, although their composite shale data remain largely invariant in $\delta^{49/47}$Ti through time (Fig. 1 and Fig. S1 in Supplementary Information). There exists a faint signal of increase in the average $\delta^{49/47}$Ti value of shales deposited from the Paleoproterozoic into the Neoproterozoic, which is also what the glacial diamictites show albeit at slightly younger (~200 Ma) depositional ages. This feature is, however, obscured in the overall scatter of the data when both individual and composite shales are plotted together. The slight temporal lag between the high $\delta^{49/47}$Ti values in individual shales and glacial diamictites can be reconciled by the fact that the depositional ages of sediments need not reflect their provenance ages.

When comparing the $\delta^{49/47}$Ti datasets, the shale data agree with the diamictite data for samples derived from the same stratigraphic unit in most cases (e.g., Witwatersrand Supergroup, Timeball Hill Formation, and Gowganda Formation). As an example, the $\delta^{49/47}$Ti values of shales from the 2.3 Ga Timeball Hill Formation (South Africa) in the Greber et al. (2017) dataset show a range from ~0.16 to 0.26‰ (Supplementary Data Table S2). Nevertheless, the Timeball Hill shale composite has a $\delta^{49/47}$Ti value of 0.24 (±0.03) ‰, indistinguishable from the $\delta^{49/47}$Ti value of the Timeball Hill diamictite composite analyzed in this study (0.22 ± 0.02‰). Klaver et al. (2021) demonstrated that the $\delta^{49/47}$Ti values of Timeball Hill shales from Greber et al. (2017) correlate positively with their Al_2O_3/TiO_2 ratios indicating a possible effect from hydrodynamic mineral sorting. Removal of Ti-bearing minerals such as Fe-Ti oxides that host isotopically light Ti could bias the fine-grained sediments towards high $\delta^{49/47}$Ti values. However, the individual Timeball Hill shale $\delta^{49/47}$Ti values are largely lower than the diamictite $\delta^{49/47}$Ti value. One possibility is that the shale $\delta^{49/47}$Ti values are affected by the concentration of biotite, a Ti-rich mineral that can incorporate isotopically light Ti at least in some cases (Greber et al., 2021). Alternatively, the positive correlation between $\delta^{49/47}$Ti and Al_2O_3/TiO_2 for the individual shales could indicate a provenance effect, with the Timeball Hill diamictite and isotopically heavier shales sampling a higher proportion of felsic rocks compared to the isotopically lighter shales. The Mozaan (Pongola) diamictite composite (South Africa) also has a higher $\delta^{49/47}$Ti value relative to a shale sample from the same unit analyzed in Greber et al. (2017) (0.21 vs 0.14‰). It is unclear to what extent these variations reflect localized provenances as opposed to processes such as hydrodynamic mineral sorting. Barring the above discrepancies, there is generally a good agreement between the average glacial diamictite $\delta^{49/47}$Ti data and the previous shale data from Greber et al. (2017) and Deng et al. (2019) for samples with similar depositional ages. This is especially true for those samples deposited in the Mesoarchean, Paleoproterozoic, and the Paleozoic. A sole exception to this includes the Neoproterozoic diamictites that carry $\delta^{49/47}$Ti values as high as 0.38‰ relative to the contemporaneous shales, which display a maximum $\delta^{49/47}$Ti value of 0.33‰ at ~ 1.0 Ga (Fig. 1). The diamictite data can be somewhat reconciled with the shale data when the broad temporal variation seen in the individual shale $\delta^{49/47}$Ti data is considered, yet the average Neoproterozoic shale $\delta^{49/47}$Ti value is lower than that of the glacial diamictites (Supplementary Data Table S2). A more detailed study of the $\delta^{49/47}$Ti compositions of Proterozoic shales is necessary to unravel whether this discrepancy reflects sampling problems within the current Proterozoic shale dataset with respect to global upper continental crust composition or relates to secondary processes such as hydrodynamic mineral sorting.

Unlike water-lain sediments such as shales, glacial diamictites are sedimentary deposits derived from physical erosion by continental ice sheets with little evidence for mineral sorting nor syn- or post-depositional weathering (Gaschnig et al., 2016; Li et al., 2016). On a $\delta^{49/47}$Ti vs Al_2O_3/TiO_2 diagram, the glacial diamictites do not show a positive correlation precluding effects related to mineral sorting (Fig. S2 in Supplementary Information). The Zr/Al_2O_3 (ppm/wt%) ratio in sediments is another sensitive indicator of hydrodynamic mineral sorting as Al_2O_3 is enriched in the fine-grained suspended mineral fraction and Zr is enriched in dense zircon grains that concentrate in the coarse-grained bedload fraction (Garçon et al., 2013; Greber and Dauphas, 2019). The $\delta^{49/47}$Ti values of glacial diamictites analysed in this study do not correlate with Zr/Al_2O_3 ratios (Fig. S2). Titanium is mainly hosted in heavy minerals such as rutile and Fe-Ti oxides that are concentrated in the coarse-sediment fraction together with zircon during hydrodynamic mineral sorting. Most diamictites analyzed in this study, with the exception of some Neoproterozoic and Paleozoic

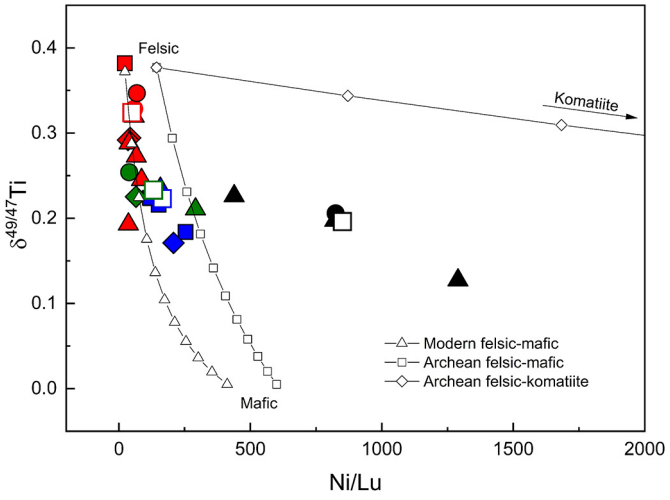

Fig. 2. The $\delta^{49/47}$Ti values of glacial diamictites plotted against their Ni/Lu ratios. The symbols are the same as in Fig. 1. Open symbols correspond to the mean of each age group. Error bars not shown for clarity. The mixing lines between felsic, mafic and komatiite end-members are calculated using the end-member compositions from Greber et al. (2017) as given in Supplementary Data Table S3. The symbols on the mixing lines indicate 10% increments in the mass fraction of the corresponding lithological end-member.

diamictites, have Zr/Al_2O_3 ratios similar to the modern upper continental crust (UCC) (Rudnick and Gao, 2014; Fig. S2). If the higher Zr/Al_2O_3 ratios in the Neoproterozoic and Paleozoic diamictites were the result of zircon concentration, they would be expected to have lower $\delta^{49/47}$Ti values due to the isotopically light nature of the Ti-bearing heavy minerals, which is not observed. In contrast, the $\delta^{49/47}$Ti values of those Neoproterozoic and Paleozoic diamictites with high Zr/Al_2O_3 ratios are largely similar to that of contemporaneous diamictites with modern UCC-like Zr/Al_2O_3 ratios. Collectively, these observations suggest that the Ti isotope record in glacial diamictites is not biased by processes such as mineral sorting and can be considered to be representative of their provenance.

3.2. Reconstruction of the upper continental crust composition

Sedimentary deposits such as glacial diamictites represent mixtures of diverse rock types exposed on Earth's surface. In order to constrain the lithological characteristics of the diamictite provenances, we estimated the relative proportions of felsic, mafic, and komatiite components that explain the measured $\delta^{49/47}$Ti values as well as selected major and trace element systematics of diamictite composites using mass balance models. This approach is necessary because Ti isotopes, on their own, cannot uniquely constrain the provenance lithology due to the differences in the Ti contents of different rock types (e.g., ~1 wt% TiO_2 in mafic rocks vs. ~0.4 wt% TiO_2 in felsic rocks; Supplementary Data Table S3). This method of quantitatively reconstructing the upper continental crust composition based on the mass balance between different lithological endmembers has been adopted in a number of recent studies (Chen et al., 2019; Greber et al., 2017; Greber and Dauphas, 2019; Ptáček et al., 2020). The robustness of this method depends upon the choice of proxy ratios that can, together with $\delta^{49/47}$Ti, be the most diagnostic of the different lithological endmembers, as well as on whether these calculations take into account the secular variations in the endmember compositions (Keller and Harrison, 2020; Ptáček et al., 2020). In this study, we primarily used the $\delta^{49/47}$Ti values in combination with Ni/Lu ratios for mass balance modelling (Fig. 2). The well-defined nature of the ternary mixing space when using $\delta^{49/47}$Ti and Ni/Lu suggests that this proxy combination can reliably distinguish between the relative proportions of felsic, mafic and komatiite rocks in the sediment provenances. A similar observation was also made by Ptacek et al. (2020), and the Ni/Lu ratio that we use is similar to the ratios found to be the most diagnostic of lithological endmembers based on an algorithmic approach in their study (e.g., Ni/Y). Furthermore, the glacial diamictite compositions plot largely within the mixing space defined by the lithological endmembers derived from the rock record for this pair, suggesting that the derived upper continental crust compositional estimates are robust. The results of our mass balance modelling suggest that the Neoproterozoic glacial diamictites on average had higher felsic rock proportions in their provenances compared to those glacial diamictites deposited in the Paleoproterozoic or in the Paleozoic (Fig. 2; Supplementary Data Table S1). This implies that the higher $\delta^{49/47}$Ti values measured in the Neoproterozoic diamictites indeed translate to a higher felsic rock proportion in their provenance.

Considering that the Ni/Lu ratio is highly sensitive to the proportion of komatiites known to affect the chemistry of at least one Paleozoic diamictite in our dataset (i.e. West Dwyka, Gaschnig et al., 2016), we also performed the mass balance modelling using ratios such as Cu/Al_2O_3 and Th/Sc which are more sensitive to mafic and felsic rock proportions respectively (Chen et al., 2019; Greber and Dauphas, 2019). Notably, the average endmember compositions from the igneous rock record (Supplementary Data Table S3) do not entirely encompass the glacial diamictite compositions for these proxy ratios even when taking the secular variations into account (Fig. S3 in Supplementary Information). These deviations likely reflect localized provenance effects, and underscore the importance of accounting for the regional scatter in sediment compositions in order to arrive at meaningful upper continental crust (UCC) compositional estimates. Despite the deviations for individual samples, the average Proterozoic and Phanerozoic glacial diamictites plot relatively close to the ternary mixing space in both $\delta^{49/47}$Ti vs. Cu/Al_2O_3 and Th/Sc diagrams suggesting the suitability of these samples for global upper continental crust studies. The same is, however, not true for the Mesoarchean glacial diamictites on the $\delta^{49/47}$Ti vs Cu/Al_2O_3 diagram. This is possibly due to the fact that Mesoarchean diamictites are derived exclusively from South Africa and may not be globally representative of the Archean upper continental crust. As a result, we preferentially focus on the Paleoproterozoic to Paleozoic diamictites in this study to reconstruct the compositional evolution of global upper continental crust across the Proterozoic Eon.

Given the divergent $\delta^{49/47}$Ti - SiO_2 trends identified for different magmatic settings (Deng et al., 2019; Hoare et al., 2020), it is possible that intraplate magmas with highly positive $\delta^{49/47}$Ti values relative to the arc magmas were predominant in the Archean Eon as a consequence of stagnant/squishy lid tectonics (Sizova et al., 2015). To determine whether intraplate magmas contributed to the chemistry of the glacial diamictites analyzed in this study, we repeated the mass balance calculations using the Ti isotope intraplate endmember and compared the results to estimates from different elemental proxies (Fig. S4 in Supplementary Information). Our results demonstrate that the lithological proportions defined by the $\delta^{49/47}$Ti intraplate endmember are inconsistent with that defined by the elemental proxies for diamictites deposited in the Proterozoic and the Phanerozoic. For the Mesoarchean diamictites, however, the coincidence of the $\delta^{49/47}$Ti arc endmember with the solution space defined by the elemental proxies breaks down. The average Mesoarchean diamictite Cu/Al_2O_3 ratio suggests a felsic rock proportion similar to that derived using the $\delta^{49/47}$Ti intraplate endmember (~15 - 30% felsic), and consistent with the vanadium isotope data for these same samples that indicate a dominantly mafic provenance (Tian et al., 2023). Nevertheless, the average Mesoarchean diamictite Cu/Al_2O_3 ratio (4.4 ± 1; Chen et al., 2019) is too high to be described by the lithological

endmembers estimated from the rock record (Fig. S3). A compilation of the Cu/Al_2O_3 ratios of shales with similar depositional ages as the Mesoarchean diamictites suggests a mean value of 2.9 (± 0.5; n=57; Supplementary Data Table S4) that is more consistent with the ternary mixing space defined by the lithological endmembers. The Archean shale Cu/Al_2O_3 ratio, in fact, defines a felsic rock proportion that agrees with that defined by the $\delta^{49/47}$Ti arc endmember and other elemental proxies (Fig. S4). Irrespective of the above uncertainty regarding the Mesoarchean upper continental crust chemical composition, it is evident that intraplate magmas did not contribute significantly to the provenances of the Proterozoic and Phanerozoic glacial diamictites that we focus on in this study. In summary, the higher $\delta^{49/47}$Ti values measured in the Neoproterozoic glacial diamictites could not have resulted from source rocks dominated by intraplate magmas and correspond to a highly felsic upper continental crust composition relative to today.

3.3. Upper crustal chemistry and the supercontinent cycle

Although deposited between ~2.4 to 2.2 Ga, the Paleoproterozoic glacial diamictites sampled crustal rocks of older Mesoarchean and Neoarchean ages as indicated by whole rock Sm-Nd and detrital zircon U-Pb data, respectively (Gaschnig et al., 2022; Mundl et al., 2018). The felsic rock fractions of up to ~80% that we estimate for the Paleoproterozoic diamictites therefore indicate a Mesoarchean to Neoarchean upper continental crust that is about as evolved as in the Phanerozoic (Fig. 3). These estimates for the Paleoproterozoic and Paleozoic diamictites are comparable to that of Greber et al. (2017), Greber and Dauphas (2019), and Ptáček et al. (2020). The Neoproterozoic glacial diamictites deposited more than a billion year later (Hofmann et al., 2015) correspond to multiple temporally distinguishable glacial events: ~717-660 Ma Sturtian, ~639-626 Ma Marinoan, and ca. 580 Ma Gaskiers (Pu et al., 2016; Rooney et al., 2015). Although deposited in the Neoproterozoic between ~0.7 to 0.6 Ga, they also sampled much older exposed continental crust as indicated by their detrital zircon U-Pb ages and Nd model ages, which date back to ~2.3 Ga (Gaschnig et al., 2022). Mass balance modelling based on convergence between multiple proxies as described earlier indicates that the Neoproterozoic diamictites sampled crustal sources with a felsic rock proportion of ~95% on average (Fig. 3 and Fig. S4). These estimates are higher than the felsic rock proportions in the modern upper continental crust (~82%; Greber and Dauphas, 2019), as well as that defined by the Paleoproterozoic and Paleozoic glacial diamictites (Fig. 3), suggesting that the overall felsic character of upper continental crust increased significantly in the Proterozoic Eon. Such a temporal variation in the upper continental crust felsic rock proportions, which has not been reported before, can be understood in the context of supercontinent assembly and dispersal cycles as described below.

The Proterozoic Eon witnessed the assembly of two supercontinents – Nuna and Rodinia. Amalgamation of most Archean cratonic blocks into the Paleoproterozoic to Mesoproterozoic supercontinent Nuna (alternately called Columbia) occurred between ~2.1 to 1.8 Ga by a series of global-scale collisional orogens (Zhao et al., 2004). There is a growing consensus today that the Nuna supercontinent underwent limited breakup in its dispersal phase and was reassembled into Rodinia between ~1.2 to 0.9 Ga without a significant reconfiguration of its core components (Cawood et al., 2016; Evans and Mitchell, 2011; Tang et al., 2021). The longevity of Nuna as one coherent supercontinent lid from the Paleoproterozoic to the Neoproterozoic ended as Rodinia broke up and the Gondwana supercontinent was assembled from its components between ~0.9 to 0.5 Ga (Meert and Lieberman, 2008). The link between the high proportions of felsic rocks recorded by the Neoproterozoic glacial diamictites and the Proterozoic supercontinent cycles be-

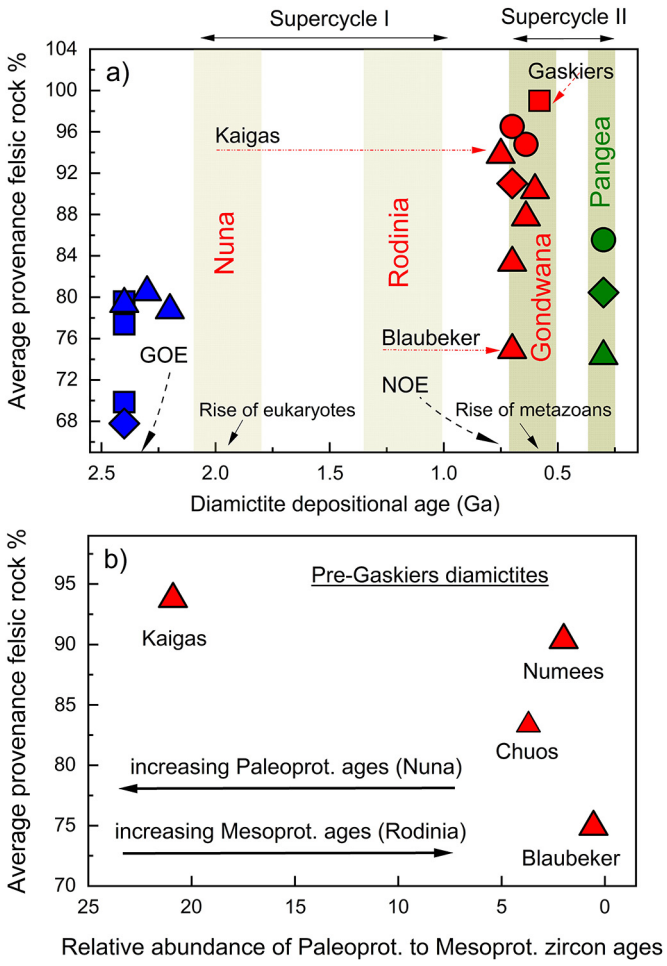

Fig. 3. The felsic rock proportions derived for the Paleoproterozoic to Paleozoic diamictites are plotted against their depositional ages in (a). Shown in (b) is the felsic rock proportions derived in this study for pre-Gaskiers diamictites from Namibia (Kaigas, Numees and Blaubeker) plotted against their average relative abundances of Paleoproterozoic to Mesoproterozoic aged zircons from Hofmann et al. (2015) and Gaschnig et al. (2022). The Proterozoic continental supercycles from Cawood et al. (2016) are shown in (a). Also shown are the time periods corresponding to the rise of eukaryotes and metazoans, as well as Great Oxidation Event (GOE) and Neoproterozoic Oxygenation Event (NOE) (Lyons et al., 2021). The symbols are the same as in Fig. 1. The arrows indicate the respective supercontinent-related crust that dominate the provenances of Kaigas, Blaubeker, Gaskiers – Nuna, Rodinia, and Gondwana respectively. Note the high felsic rock proportions in Kaigas and Gaskiers, corresponding to Nuna and Gondwana orogeny, and separated by an orogenic quiescence related to the Nuna-Rodinia continental supercycle (Cawood et al., 2016).

comes evident when the disparate diamictite provenance ages, as defined by zircon U-Pb geochronology, are considered. For example, the Neoproterozoic diamictite Kaigas (Namibia) which records a high felsic rock proportion of ~94% in our study has an essentially unimodal ~1.9 Ga zircon U-Pb age peak (Gaschnig et al., 2022; Hofmann et al., 2015). This suggests that the Kaigas diamictite, though deposited in the Neoproterozoic, predominantly sampled a mid-Paleoproterozoic source that consisted almost entirely of felsic rocks. Prevalence of a highly felsic upper continental crust at ca. 1.9 Ga, compared to the late Archean or early Paleoproterozoic when the felsic rock proportions were at most ~80%, can be attributed to the collisional amalgamation of the Nuna supercontinent (Fig. 3a). Given the intimate association between continental collisions, crustal thickening, and felsic magmatism via increased degrees of magma differentiation and crustal melting (Searle, 2013; Ducea et al., 2015), the collisional assembly of Nuna between ~2.1 to 1.8 Ga nicely explains the highly felsic character of the Kaigas diamictite provenance. It is possible that formation of

the Nuna supercontinent represents the earliest instance in terrestrial history when collisional orogens with high topographic relief became a feature of Earth's surface. Although continents emerged above the sea level several hundred million years earlier (Bindeman et al., 2018; Roerdink et al., 2022), they are unlikely to have had a topographic relief as high as the Nuna mountains given the less felsic character of the upper continental crust sampled by the Paleoproterozoic glacial diamictites.

The ~1.9 Ga zircon U-Pb age peak related to Nuna assembly is a common feature of detrital zircons from most Namibian Neoproterozoic diamictites in our dataset, in addition to another major protracted peak between ~1.4 to 1.0 Ga (Gaschnig et al., 2022; Hofmann et al., 2015). The second peak is similar to the Mesoproterozoic peak seen globally in detrital zircon data corresponding to the assembly of the Rodinia supercontinent (Condie et al., 2009). This suggests that the Namibian diamictites, with the exception of Kaigas, sampled crust related to both Nuna and Rodinia assembly, albeit at considerably different proportions. For instance, Blaubeker which records the lowest felsic rock proportions amongst the Neoproterozoic diamictites (~75%) has a dominant Mesoproterozoic zircon population in sharp contrast to Kaigas (Gaschnig et al., 2022; Hofmann et al., 2014, 2015). This is demonstrated in Fig. 3b where the relative abundance of Paleoproterozoic to Mesoproterozoic zircons in the Namibian diamictites compiled from the literature is plotted against the felsic rock proportions in their provenance estimated here. The Numees and Chuos diamictites, which record intermediate proportions of felsic rocks of ~80 - 90% fall between Kaigas and Blaubeker in their relative abundance of Paleoproterozoic to Mesoproterozoic zircons. This broad relationship indicates that the Mesoproterozoic crust related to Rodinia assembly consisted of a lower felsic rock proportion, by as much as ~20% or more, compared to the Nuna-related mid-Paleoproterozoic crust. The Neoproterozoic Gucheng and Nantuo diamictites from Yangtze Block (China) which record high proportions of felsic rocks of ~95% also have dominant Paleoproterozoic detrital zircon populations and a notable absence of detrital zircons with Mesoproterozoic ages (Liu et al., 2008). The apparent decrease in the felsic rock proportions of upper continental crust while going from ~1.9 to ~1.2 Ga is likely related to the Nuna-Rodinia continental super cycle (Cawood et al., 2016). The long-lived nature of Nuna orogenic belts that imply minimal paleogeographic changes across the transition to Rodinia (Evans and Mitchell, 2011), as well as the evidence for Rodinia assembly by introversion (Cawood et al., 2016; Li et al., 2008), collectively suggest that continental collisions were limited during the formation of the Rodinia supercontinent.

Breakup of Rodinia commenced between ~0.9 - 0.7 Ga by the development of peripheral accretionary orogens (Cawood et al., 2016), ultimately leading to its reassembly into the Gondwana supercontinent (Meert and Lieberman, 2008). Paleogeographic reconstructions suggest that the main phase of Gondwana assembly between ~0.6 - 0.5 Ga involved a complete reconfiguration of Rodinia by a series of continent-continent collisions (Cawood et al., 2016; Meert and Lieberman, 2008). Given the evidence for deep subduction of continental crust starting at ca. 620 Ma (Ganade de Araujo et al., 2014), it has been proposed that Himalayan-style mountain belts with high topographic relief were ubiquitous at this time. In line with this hypothesis, we note that the Gaskiers diamictite (Canada) that has a largely unimodal ~650 - 550 Ma zircon U-Pb age spectrum (Gaschnig et al., 2022) defines the highest felsic rock proportions estimated in this study (~99%; Fig. 3a). The highly felsic nature of the Gaskiers diamictite provenance can be attributed to the collisional mountain-building associated with Gondwana supercontinent assembly. The orogenic quiescence related to the Nuna-Rodinia continental supercycle (Tang et al., 2021) was thus terminated by the assembly of the Gondwana supercontinent, as reflected in the highly felsic ~0.6 Ga provenance of the Gaskiers diamictite in our dataset (Fig. 3a). This emerging picture of the Proterozoic crustal evolution is consistent with Zhu et al. (2022) who suggested that the assembly of Nuna and Gondwana supercontinents represents the two periods in terrestrial history that correspond to high relief (Himalayan-type) supermountain formation. The distribution of detrital low-Lu zircons, which Zhu et al. (2022) used as a proxy for high-pressure metamorphism related to collisional orogenesis, shows a clear bimodality with peaks corresponding to Nuna and Gondwana supercontinents (Zhu et al., 2022). Our results echo a similar temporal distribution for upper continental crust felsic rock proportions, with Kaigas and Gaskiers diamictites, respectively, representing the highly felsic crust associated with ~1.9 Ga Nuna and ~0.6 Ga Gondwana assembly. The intervening assembly of Rodinia evidently did not result in the formation of high relief mountains given the lack of a low-Lu detrital zircon peak at this time (Zhu et al., 2022), crustal thickness minimum recorded in zircons of Rodinian ages (Tang et al., 2021), and the lower felsic rock proportions in the Blaubeker diamictite provenance corresponding to the Mesoproterozoic upper continental crust (Fig. 3b).

In contrast to the results presented here, several studies have previously argued that the average felsic nature of continents did not change significantly through time (Garçon, 2021; Greber et al., 2017; Ptáček et al., 2020). The shale data from Greber et al. (2017) can be somewhat reconciled with the glacial diamictite data in this study as discussed in section 3.1. Although the reconstructed upper continental crust SiO_2 contents in Ptáček et al. (2020) remain relatively invariant through time, the estimated felsic rock proportions show variations between ca. 2 Ga and 0.5 Ga that mirror our results in some cases (cf. Fig 5; Ptáček et al. (2020)). The agreement between the two studies is largely dependent on the use of proxy ratios that are the most diagnostic of crustal endmembers (e.g., Ni/Y). The study of Garçon (2021) used the $^{147}Sm/^{144}Nd$ ratios of sedimentary rocks to reconstruct the average continental crust SiO_2 content. However, the $^{147}Sm/^{144}Nd$ ratio is largely insenstiive to the SiO_2 content beyond ~65 wt% SiO_2 implying that this approach might be less suited to explore the compositoinal evolution associated with crustal thickening and melting. Notably, most of the Neoproterozoic glacial diamictites analysed in this study with the exception of Blaubeker have reconstructed provenance SiO_2 contents between ~ 67 to 71 wt% (Supplementary Data Table S5). Moreover, our results show a good agreement with Lipp et al. (2021) who used a vector-based approach based on the major element composition of sediments to reconstruct the protolith composition. Lipp et al. (2021) demonstrates an increase in the average SiO_2 content of the sediment protoliths between ~ 2 to 0.5 Ga compared to before and after, similar to the results of this study. Lastly, vanadium isotope data from Tian et al. (2023) for the same glacial diamictite composites analyzed in this study broadly agree with our results, with Kaigas and Gaskiers recording the highest silica contents of all glacial diamictites in their provenance (cf. Table S2; Tian et al., 2023).

3.4. Tectonics, oxygenation, and biological evolution

The Neoproterozoic eon that witnessed the assembly of the Gondwana supercontinent is a period of great upheaval for Earth's oceans, atmosphere, and biosphere. There may have been sufficient oxygen in the atmosphere to ventilate the surface ocean since the GOE (Holland, 2002), but evidence for deep prolific ocean oxygenation exists only since the late Neoproterozoic, which likely facilitated the rise of animal life (Canfield et al., 2007; Sahoo et al., 2012). Nevertheless, an alternative view holds that deep ocean oxygenation was likely limited or transient at this time, cautioning against inferring a direct cause-and-effect relationship between

marine redox changes and rise of animals (Sperling et al., 2015). Regardless of whether global ocean oxygenation enabled or followed the emergence of animal life, it is universally acknowledged that the global carbon cycle underwent significant perturbations at this time, suggesting release of oxidising power at least to the surface environment since ~800 Ma (Och and Shields-Zhou, 2012). The results presented in this study support the hypothesis that the increased nutrient supply required to explain the Neoproterozoic redox changes was primarily derived from erosion of high-relief Gondwana mountains (Campbell and Allen, 2008; Campbell and Squire, 2010; Ganade de Araujo et al., 2014; Zhu et al., 2022). Although enhanced nutrient loading into oceans in the aftermath of the Neoproterozoic 'snowball' Earth glaciations could have occurred (Sahoo et al., 2012), post-glacial fluxes are likely transient events with durations of less than a million year (Zhou et al., 2019). Denudation of collisional orogens such as Gondwana that take place over 10-100 Myr timescales provide a more sustained erosional flux from continents to oceans (Song et al., 2015). The increased continental erosion associated with Gondwana mountains is also reflected in the distinct peak in seawater strontium isotopes seen at this time (Shields, 2007).

The profound changes in the Neoproterozoic Earth System appear to have operated in phase with Gondwana assembly, after an ~1-billion-year hiatus in collisional orogenesis since Nuna assembly. Specifically, nutrient throttling that likely maintained muted levels of ocean productivity and surface oxygen for most of the mid-Proterozoic (Anbar and Knoll, 2002) appears to have been efficiently overcome with the advent of Gondwana orogeny. Enhanced nutrient availability, especially of phosphorous, could have initiated a more active marine biological realm that drove net oxygen release to the atmosphere and facilitated the evolution of larger, complex Ediacaran biota (Brocks et al., 2017). In this framework, it is noteworthy that the period of Nuna assembly – the first known instance when collisional mountain belts dominated Earth's topography, and with their erosion likely enhancing the nutrient supply into oceans – coincides with the key evolutionary transition from prokaryotic to eukaryotic organisms (Butterfield, 2015). Multiple molecular clock analyses indicate that the last eukaryotic common ancestor emerged by ~1900 to 1700 Ma (Betts et al., 2018; Parfrey et al., 2011), exhibiting a remarkable temporal correlation with Nuna supercontinent assembly (Zhao et al., 2004). The temporal correlation between the Paleoproterozoic biological innovations and the erosional supply from Nuna mountains is also evident in the first discernible peak recorded in seawater strontium isotopes at this time (Shields, 2007). Furthermore, the period of Nuna assembly coincides with the earliest unambiguous fossil record of cyanobacteria – the only prokaryotic organisms that developed the ability to perform oxygenic photosynthesis (Demoulin et al., 2019). Although their stem lineages likely evolved much earlier in the Archean, cyanobacteria reached their maximum morphological complexity roughly around the same time the first eukaryotes evolved (Betts et al., 2018; Demoulin et al., 2019). This overall pattern of development of complexity for both prokaryotes and eukaryotes could indicate that marine nutrient availability that varied in response to collisional mountain-building likely exerted a significant control on the diversification of life and associated macroevolutionary lags.

Surges in marine nutrient supply have been previously linked to greater trophic complexity and predation in planktonic ecosystems explaining the time lag between the origin of eukaryotes and their delayed rise to ecological dominance (Brocks et al., 2017; Reinhard et al., 2020). This likely set the stage for the subsequent evolution of the Ediacaran biota (Narbonne, 2004). However, such a bottom-up control has not yet been proposed for the radiation of early eukaryotes from dominantly prokaryotic ecosystems. Additionally, the Paleoproterozoic origin of eukaryotes has not been shown to be closely accompanied by a significant rise in atmospheric oxygen as with the Neoproterozoic eukaryote diversification and radiation of metazoans. Exactly how an enhanced marine nutrient inventory, correlated to the erosion of Nuna mountains, could have paved the way for the radiation of eukaryotes is an exciting avenue of future research. Factors such as resource availability facilitating larger size classes, and removal of environmental constraints (e.g. oxygen) allowing for biological innovations could have been important (Irwin et al., 2006; Payne et al., 2009). Alternatively, there might have been small-scale changes in surface oxygen levels associated with Nuna erosion that targeted investigations could unravel (Zhu et al., 2022). An example here is the disappearance of banded iron formations at ca. 1.8 Ga traditionally linked to the oxidation of dissolved iron (Holland, 2006), although alternate explanations exist (Poulton et al., 2010). Regardless of the exact mechanism, the step changes in the evolution of organismal complexity over terrestrial history appear to be temporally correlated to instances of enhanced nutrient supply from continents to oceans via collisional mountain-building and generation of high continental topography (Zhu et al., 2022). The availability of bio-essential nutrients in the Proterozoic oceans possibly varied as a function of collisional mountain-building, with important plausible consequences for the trajectory of life from prokaryotes to eukaryotes, and eventually metazoans. Future studies that look into the role of plate tectonics in modulating the oceanic availability of biologically important nutrients through deep time, especially in the Paleoproterozoic, and a richer mechanistic understanding of the complex interplay between nutrient availability, ecological hierarchies, surface oxygenation, and organismal complexity are imperative.

4. Conclusions

Titanium isotope signatures in glacial diamictites, when combined with elemental data, document a significant variation in the felsic character of upper continental crust across the Proterozoic eon. Previously reported titanium isotope data for shales can be reconciled with the glacial diamictite data to a large extent. Nevertheless, the Neoproterozoic shale $\delta^{49/47}$Ti values are lower than that measured for the contemporaneous diamictites in this study. The upper continental crust lithological variations evident in the glacial diamictite data can be explained in terms of continental collisions that result in high topography and permit increased degrees of crustal melting and magma differentiation. In particular, the high continental topography inferred from the highly felsic upper continental crust compositions recorded in glacial diamictites corresponds to the collisional assembly of Nuna and Gondwana supercontinents at ~ 2.1 - 1.8 Ga and ~ 0.7 - 0.5 Ga respectively. There exists a remarkable temporal correlation between the periods of high continental topography and the key transitions in the trajectory of life from prokaryotes to eukaryotes, and eventually metazoans. The intervening period during which biological evolution largely stalled was marked by the long-lived Nuna-Rodinia continental supercycle and a paucity of continental collisions. We speculate that the continental supply of nutrients to oceans modulated by plate tectonics likely exerted a significant control on the levels of biological and ecological organization over terrestrial history.

CRediT authorship contribution statement

R.L.R. and M.A.M. conceived the project. R.M.G. collected and characterized the samples. N.S.S. performed the data acquisition and analysis. N.S.S., R.L.R., R.M.G., and M.A.M shared in the interpretation, and N.S.S. wrote the manuscript. All authors contributed to editing and finalizing the manuscript.

Declaration of competing interest

The authors declare no competing interests.

Data availability

Data will be made available on request.

Acknowledgements

We thank Morten B. Andersen for insightful discussions and comments that greatly improved this work, Ernest C. Fru for feedback on an earlier version of this manuscript, Boswell Wing for editorial handling, and Oliver Nebel and an anonymous reviewer for their constructive comments. Anabel Morte-Rodenas and Lindsey Owen are acknowledged for support in the laboratory. This study was funded by a NERC standard grant (NE/R001332/1) to M.A.M and NSF grant EAR-1321954 to RLR and RMG.

Appendix A. Supplementary material

Supplementary material related to this article can be found online at https://doi.org/10.1016/j.epsl.2023.118214.

References

Anbar, A.D., Knoll, A.H., 2002. Proterozoic ocean chemistry and evolution: a bioinorganic bridge? Science 297 (5584), 1137–1142. https://doi.org/10.1126/science.1069651.

Betts, H.C., Puttick, M.N., Clark, J.W., Williams, T.A., Donoghue, P.C.J., Pisani, D., 2018. Integrated genomic and fossil evidence illuminates life's early evolution and eukaryote origin. Nat. Ecol. Evol. 2 (10), 1556–1562. https://doi.org/10.1038/s41559-018-0644-x.

Bindeman, I.N., Zakharov, D.O., Palandri, J., Greber, N.D., Dauphas, N., Retallack, G.J., Hofmann, A., Lackey, J.S., Bekker, A., 2018. Rapid emergence of subaerial landmasses and onset of a modern hydrologic cycle 2.5 billion years ago. Nature 557 (7706), 545–548. https://doi.org/10.1038/s41586-018-0131-1.

Brocks, J.J., Jarrett, A.J.M., Sirantoine, E., Hallmann, C., Hoshino, Y., Liyanage, T., 2017. The rise of algae in Cryogenian oceans and the emergence of animals. Nature 548 (7669), 578–581. https://doi.org/10.1038/nature23457.

Butterfield, N.J., 2015. Early evolution of the Eukaryota. Palaeontology 58 (1), 5–17. https://doi.org/10.1111/pala.12139.

Campbell, I.H., Allen, C.M., 2008. Formation of supercontinents linked to increases in atmospheric oxygen. Nat. Geosci. 1 (8), 554–558. https://doi.org/10.1038/ngeo259.

Campbell, I.H., Squire, R.J., 2010. The mountains that triggered the late neoproterozoic increase in oxygen: the second great oxidation event. Geochim. Cosmochim. Acta 74 (15), 4187–4206. https://doi.org/10.1016/j.gca.2010.04.064.

Canfield, D.E., Poulton, S.W., Narbonne, G.M., 2007. Late-neoproterozoic deep-ocean oxygenation and the rise of animal life. Science 315 (5808), 92. https://doi.org/10.1126/science.1135013.

Cawood, P.A., Strachan, R.A., Pisarevsky, S.A., Gladkochub, D.P., Murphy, J.B., 2016. Linking collisional and accretionary orogens during Rodinia assembly and breakup: implications for models of supercontinent cycles. Earth Planet. Sci. Lett. 449, 118–126. https://doi.org/10.1016/j.epsl.2016.05.049.

Chen, K., Rudnick, R.L., Wang, Z., Tang, M., Gaschnig, R.M., Zou, Z., He, T., Hu, Z., Liu, Y., 2019. How mafic was the Archean upper continental crust? Insights from Cu and Ag in ancient glacial diamictites. Geochim. Cosmochim. Acta. https://doi.org/10.1016/J.GCA.2019.08.002.

Condie, K.C., Belousova, E., Griffin, W.L., Sircombe, K.N., 2009. Granitoid events in space and time: constraints from igneous and detrital zircon age spectra. Gondwana Res. 15 (3), 228–242. https://doi.org/10.1016/j.gr.2008.06.001.

Demoulin, C.F., Lara, Y.J., Cornet, L., François, C., Baurain, D., Wilmotte, A., Javaux, E.J., 2019. Cyanobacteria evolution: insight from the fossil record. Free Radic. Biol. Med. 140, 206–223. https://doi.org/10.1016/j.freeradbiomed.2019.05.007.

Deng, Z., Chaussidon, M., Savage, P., Robert, F., Pik, R., Moynier, F., 2019. Titanium isotopes as a tracer for the plume or island arc affinity of felsic rocks. Proc. Natl. Acad. Sci. 116 (4), 1132. https://doi.org/10.1073/pnas.1809164116.

Dewey, J.F., Bird, J.M., 1970. Mountain belts and the new global tectonics. J. Geophys. Res. (1896–1977) 75 (14), 2625–2647. https://doi.org/10.1029/JB075i014p02625.

Ducea, M.N., Saleeby, J.B., Bergantz, G., 2015. The architecture, chemistry, and evolution of continental magmatic arcs. Annu. Rev. Earth Planet. Sci. 43 (1), 299–331. https://doi.org/10.1146/annurev-earth-060614-105049.

Evans, D.A.D., Mitchell, R.N., 2011. Assembly and breakup of the core of Paleoproterozoic–Mesoproterozoic supercontinent Nuna. Geology 39 (5), 443–446. https://doi.org/10.1130/G31654.1.

Galy, A., France-Lanord, C., 2001. Higher erosion rates in the Himalaya: geochemical constraints on riverine fluxes. Geology 29 (1), 23–26. https://doi.org/10.1130/0091-7613(2001)029<0023:HERITH>2.0.CO;2.

Ganade de Araujo, C.E., Rubatto, D., Hermann, J., Cordani, U.G., Caby, R., Basei, M.A.S., 2014. Ediacaran 2,500-km-long synchronous deep continental subduction in the West Gondwana Orogen. Nat. Commun. 5 (1), 5198. https://doi.org/10.1038/ncomms6198.

Garçon, M., 2021. Episodic growth of felsic continents in the past 3.7 Ga. Sci. Adv. 7 (39), eabj1807. https://doi.org/10.1126/sciadv.abj1807.

Garçon, M., Chauvel, C., France-Lanord, C., Huyghe, P., Lavé, J., 2013. Continental sedimentary processes decouple Nd and Hf isotopes. Geochim. Cosmochim. Acta 121, 177–195. https://doi.org/10.1016/j.gca.2013.07.027.

Gaschnig, R.M., Horan, M.F., Rudnick, R.L., Vervoort, J.D., Fisher, C.M., 2022. History of crustal growth in Africa and the Americas from detrital zircon and Nd isotopes in glacial diamictites. Precambrian Res. 373, 106641. https://doi.org/10.1016/j.precamres.2022.106641.

Gaschnig, R.M., Rudnick, R.L., McDonough, W.F., Kaufman, A.J., Hu, Z., Gao, S., 2014. Onset of oxidative weathering of continents recorded in the geochemistry of ancient glacial diamictites. Earth Planet. Sci. Lett. 408, 87–99. https://doi.org/10.1016/J.EPSL.2014.10.002.

Gaschnig, R.M., Rudnick, R.L., McDonough, W.F., Kaufman, A.J., Valley, J.W., Hu, Z., Gao, S., Beck, M.L., 2016. Compositional evolution of the upper continental crust through time, as constrained by ancient glacial diamictites. Geochim. Cosmochim. Acta 186, 316–343. https://doi.org/10.1016/J.GCA.2016.03.020.

Greber, N.D., Dauphas, N., 2019. The chemistry of fine-grained terrigenous sediments reveals a chemically evolved Paleoarchean emerged crust. Geochim. Cosmochim. Acta 255, 247–264. https://doi.org/10.1016/J.GCA.2019.04.012.

Greber, N.D., Dauphas, N., Bekker, A., Ptáček, M.P., Bindeman, I.N., Hofmann, A., 2017. Titanium isotopic evidence for felsic crust and plate tectonics 3.5 billion years ago. Science 357 (6357), 1271–1274. https://doi.org/10.1126/science.aan8086.

Greber, N.D., Pettke, T., Vilela, N., Lanari, P., Dauphas, N., 2021. Titanium isotopic compositions of bulk rocks and mineral separates from the Kos magmatic suite: insights into fractional crystallization and magma mixing processes. Chem. Geol. 578, 120303. https://doi.org/10.1016/j.chemgeo.2021.120303.

Hoare, L., Klaver, M., Saji, N.S., Gillies, J., Parkinson, I.J., Lissenberg, C.J., Millet, M.A., 2020. Melt chemistry and redox conditions control titanium isotope fractionation during magmatic differentiation. Geochim. Cosmochim. Acta 282, 38–54. https://doi.org/10.1016/j.gca.2020.05.015.

Hofmann, M., Linnemann, U., Hoffmann, K.-H., Gerdes, A., Eckelmann, K., Gärtner, A., 2014. The Namuskluft and Dreigratberg sections in southern Namibia (Kalahari Craton, Gariep Belt): a geological history of Neoproterozoic rifting and recycling of cratonic crust during the dispersal of Rodinia until the amalgamation of Gondwana. Int. J. Earth Sci. 103 (5), 1187–1202. https://doi.org/10.1007/s00531-013-0949-6.

Hofmann, M., Linnemann, U., Hoffmann, K.-H., Germs, G., Gerdes, A., Marko, L., Eckelmann, K., Gärtner, A., Krause, R., 2015. The four Neoproterozoic glaciations of southern Namibia and their detrital zircon record: the fingerprints of four crustal growth events during two supercontinent cycles. Precambrian Res. 259, 176–188. https://doi.org/10.1016/j.precamres.2014.07.021.

Holland, H.D., 2002. Volcanic gases, black smokers, and the great oxidation event. Geochim. Cosmochim. Acta 66 (21), 3811–3826. https://doi.org/10.1016/S0016-7037(02)00950-X.

Holland, H.D., 2006. The oxygenation of the atmosphere and oceans. Philosophical Transactions of the Royal Society B: Biological Sciences 361 (1470), 903–915. https://doi.org/10.1098/rstb.2006.1838.

Hopkinson, T.N., Harris, N.B.W., Warren, C.J., Spencer, C.J., Roberts, N.M.W., Horstwood, M.S.A., Parrish, R.R., EIMF, 2017. The identification and significance of pure sediment-derived granites. Earth Planet. Sci. Lett. 467, 57–63. https://doi.org/10.1016/j.epsl.2017.03.018.

Irwin, A.J., Finkel, Z.V., Schofield, O.M.E., Falkowski, P.G., 2006. Scaling-up from nutrient physiology to the size-structure of phytoplankton communities. J. Plankton Res. 28 (5), 459–471. https://doi.org/10.1093/plankt/fbi148.

Johnson, A.C., Aarons, S.M., Dauphas, N., Nie, N.X., Zeng, H., Helz, R.T., Romaniello, S.J., Anbar, A.D., 2019. Titanium isotopic fractionation in Kilauea Iki lava lake driven by oxide crystallization. Geochim. Cosmochim. Acta 264, 180–190. https://doi.org/10.1016/J.GCA.2019.08.022.

Keller, C.B., Harrison, T.M., 2020. Constraining crustal silica on ancient Earth. Proc. Natl. Acad. Sci. 117 (35), 21101–21107. https://doi.org/10.1073/pnas.2009431117.

Klaver, M., MacLennan, S.A., Ibañez-Mejia, M., Tissot, F.L.H., Vroon, P.Z., Millet, M.-A., 2021. Reliability of detrital marine sediments as proxy for continental crust composition: the effects of hydrodynamic sorting on Ti and Zr isotope systematics. Geochim. Cosmochim. Acta. https://doi.org/10.1016/j.gca.2021.05.030.

Lenardic, A., Jellinek, A.M., Foley, B., O'Neill, C., Moore, W.B., 2016. Climate-tectonic coupling: variations in the mean, variations about the mean, and variations in mode. J. Geophys. Res., Planets 121 (10), 1831–1864. https://doi.org/10.1002/2016JE005089.

Li, S., Gaschnig, R.M., Rudnick, R.L., 2016. Insights into chemical weathering of the upper continental crust from the geochemistry of ancient glacial diamictites. Geochim. Cosmochim. Acta 176, 96–117. https://doi.org/10.1016/J.GCA.2015.12.012.

Li, Z.X., Bogdanova, S.V., Collins, A.S., Davidson, A., De Waele, B., Ernst, R.E., Fitzsimons, I.C.W., Fuck, R.A., Gladkochub, D.P., Jacobs, J., Karlstrom, K.E., Lu, S., Natapov, L.M., Pease, V., Pisarevsky, S.A., Thrane, K., Vernikovsky, V., 2008. Assembly, configuration, and break-up history of Rodinia: a synthesis. Precambrian Res. 160 (1), 179–210. https://doi.org/10.1016/j.precamres.2007.04.021.

Lipp, A.G., Shorttle, O., Sperling, E.A., Brocks, J.J., Cole, D.B., Crockford, P.W., Mouro, L. Del, Dewing, K., Dornbos, S.Q., Emmings, J.F., Farrell, U.C., Jarrett, A., Johnson, B.W., Kabanov, P., Keller, C.B., Kunzmann, M., Miller, A.J., Mills, N.T., O'Connell, B., Yang, J., et al., 2021. The composition and weathering of the continents over geologic time. Geochem. Perspect. Lett. 17, 21–26. https://doi.org/10.7185/geochemlet.2109.

Liu, X., Gao, S., Diwu, C., Ling, W., 2008. Precambrian crustal growth of Yangtze Craton as revealed by detrital zircon studies. Am. J. Sci. 308 (4), 421–468. https://doi.org/10.2475/04.2008.02.

Lyons, T.W., Diamond, C.W., Planavsky, N.J., Reinhard, C.T., Li, C., 2021. Oxygenation, life, and the planetary system during Earth's middle history: an overview. Astrobiology 21 (8), 906–923. https://doi.org/10.1089/ast.2020.2418.

Marais, D.J. Des, Strauss, H., Summons, R.E., Hayes, J.M., 1992. Carbon isotope evidence for the stepwise oxidation of the Proterozoic environment. Nature 359 (6396), 605–609. https://doi.org/10.1038/359605a0.

Meert, J.G., Lieberman, B.S., 2008. The Neoproterozoic assembly of Gondwana and its relationship to the Ediacaran–Cambrian radiation. Gondwana Res. 14 (1), 5–21. https://doi.org/10.1016/j.gr.2007.06.007.

Millet, M.-A., Dauphas, N., 2014. Ultra-precise titanium stable isotope measurements by double-spike high resolution MC-ICP-MS. J. Anal. At. Spectrom. 29 (8), 1444–1458. https://doi.org/10.1039/C4JA00096J.

Millet, M.-A., Dauphas, N., Greber, N.D., Burton, K.W., Dale, C.W., Debret, B., Macpherson, C.G., Nowell, G.M., Williams, H.M., 2016. Titanium stable isotope investigation of magmatic processes on the Earth and Moon. Earth Planet. Sci. Lett. 449, 197–205. https://doi.org/10.1016/J.EPSL.2016.05.039.

Mundl, A., Walker, R.J., Reimink, J.R., Rudnick, R.L., Gaschnig, R.M., 2018. Tungsten-182 in the upper continental crust: evidence from glacial diamictites. Chem. Geol. 494, 144–152. https://doi.org/10.1016/j.chemgeo.2018.07.036.

Narbonne, G.M., 2004. The Ediacara Biota: Neoproterozoic origin of animals and their ecosystems. Annu. Rev. Earth Planet. Sci. 33 (1), 421–442. https://doi.org/10.1146/annurev.earth.33.092203.122519.

Nursall, J.R., 1959. Oxygen as a prerequisite to the origin of the metazoa. Nature 183 (4669), 1170–1172. https://doi.org/10.1038/1831170b0.

Och, L.M., Shields-Zhou, G.A., 2012. The Neoproterozoic oxygenation event: environmental perturbations and biogeochemical cycling. Earth-Sci. Rev. 110 (1), 26–57. https://doi.org/10.1016/j.earscirev.2011.09.004.

Parfrey, L.W., Lahr, D.J.G., Knoll, A.H., Katz, L.A., 2011. Estimating the timing of early eukaryotic diversification with multigene molecular clocks. Proc. Natl. Acad. Sci. 108 (33), 13624–13629. https://doi.org/10.1073/pnas.1110633108.

Payne, J.L., Boyer, A.G., Brown, J.H., Finnegan, S., Kowalewski, M., Krause, R.A., Lyons, S.K., McClain, C.R., McShea, D.W., Novack-Gottshall, P.M., Smith, F.A., Stempien, J.A., Wang, S.C., 2009. Two-phase increase in the maximum size of life over 3.5 billion years reflects biological innovation and environmental opportunity. Proc. Natl. Acad. Sci. 106 (1), 24–27. https://doi.org/10.1073/pnas.0806314106.

Poulton, S.W., Fralick, P.W., Canfield, D.E., 2010. Spatial variability in oceanic redox structure 1.8 billion years ago. Nat. Geosci. 3 (7), 486–490. https://doi.org/10.1038/ngeo889.

Ptáček, M.P., Dauphas, N., Greber, N.D., 2020. Chemical evolution of the continental crust from a data-driven inversion of terrigenous sediment compositions. Earth Planet. Sci. Lett. 539, 116090. https://doi.org/10.1016/j.epsl.2020.116090.

Pu, J.P., Bowring, S.A., Ramezani, J., Myrow, P., Raub, T.D., Landing, E., Mills, A., Hodgin, E., Macdonald, F.A., 2016. Dodging snowballs: geochronology of the Gaskiers glaciation and the first appearance of the Ediacaran biota. Geology 44 (11), 955–958. https://doi.org/10.1130/G38284.1.

Reinhard, C.T., Planavsky, N.J., Ward, B.A., Love, G.D., Le Hir, G., Ridgwell, A., 2020. The impact of marine nutrient abundance on early eukaryotic ecosystems. Geobiology 18 (2), 139–151. https://doi.org/10.1111/gbi.12384.

Roerdink, D.L., Ronen, Y., Strauss, H., Mason, P.R.D., 2022. Emergence of felsic crust and subaerial weathering recorded in Palaeoarchaean barite. Nat. Geosci. 15 (3), 227–232. https://doi.org/10.1038/s41561-022-00902-9.

Rooney, A.D., Strauss, J.V., Brandon, A.D., Macdonald, F.A., 2015. A Cryogenian chronology: two long-lasting synchronous Neoproterozoic glaciations. Geology 43 (5), 459–462. https://doi.org/10.1130/G36511.1.

Rudnick, R.L., Gao, S., 2014. Composition of the Continental Crust. Treatise on Geochemistry, pp. 1–51.

Sahoo, S.K., Planavsky, N.J., Kendall, B., Wang, X., Shi, X., Scott, C., Anbar, A.D., Lyons, T.W., Jiang, G., 2012. Ocean oxygenation in the wake of the Marinoan glaciation. Nature 489 (7417), 546–549. https://doi.org/10.1038/nature11445.

Searle, M., 2013. Crustal melting, ductile flow, and deformation in mountain belts: cause and effect relationships. Lithosphere 5 (6), 547–554. https://doi.org/10.1130/RF.L006.1.

Shields, G.A., 2007. A normalised seawater strontium isotope curve: possible implications for Neoproterozoic-Cambrian weathering rates and the further oxygenation of the Earth. EEarth 2 (2), 35–42. https://doi.org/10.5194/ee-2-35-2007.

Sizova, E., Gerya, T., Stüwe, K., Brown, M., 2015. Generation of felsic crust in the Archean: a geodynamic modeling perspective. Precambrian Res. 271, 198–224. https://doi.org/10.1016/J.PRECAMRES.2015.10.005.

Song, S., Wang, M., Wang, C., Niu, Y., 2015. Magmatism during continental collision, subduction, exhumation and mountain collapse in collisional orogenic belts and continental net growth: a perspective. Sci. China Earth Sci. 58 (8), 1284–1304. https://doi.org/10.1007/s11430-015-5102-x.

Sperling, E.A., Wolock, C.J., Morgan, A.S., Gill, B.C., Kunzmann, M., Halverson, G.P., Macdonald, F.A., Knoll, A.H., Johnston, D.T., 2015. Statistical analysis of iron geochemical data suggests limited late Proterozoic oxygenation. Nature 523 (7561), 451–454. https://doi.org/10.1038/nature14589.

Tang, M., Xu, C., Jihua, H., Bing, S., 2021. Orogenic quiescence in Earth's middle age. Science 371 (6530), 728–731. https://doi.org/10.1126/science.abf1876.

Tian, S., Ding, X., Qi, Y., Wu, F., Cai, Y., Gaschnig, R.M., Xiao, Z., Lv, W., Rudnick, R.L., Huang, F., 2023. Dominance of felsic continental crust on Earth after 3 billion years ago is recorded by vanadium isotopes. Proc. Natl. Acad. Sci. 120 (11), e2220563120. https://doi.org/10.1073/pnas.2220563120.

Walker, J.C.G., Hays, P.B., Kasting, J.F., 1981. A negative feedback mechanism for the long-term stabilization of Earth's surface temperature. J. Geophys. Res., Oceans 86 (C10), 9776–9782. https://doi.org/10.1029/JC086iC10p09776.

Zhang, J., Dauphas, N., Davis, A.M., Pourmand, A., 2011. A new method for MC-ICPMS measurement of titanium isotopic composition: identification of correlated isotope anomalies in meteorites. J. Anal. At. Spectrom. 26 (11), 2197–2205. https://doi.org/10.1039/C1JA10181A.

Zhao, G., Sun, M., Wilde, S.A., Li, S., 2004. A Paleo-Mesoproterozoic supercontinent: assembly, growth and breakup. Earth-Sci. Rev. 67 (1), 91–123. https://doi.org/10.1016/j.earscirev.2004.02.003.

Zhou, C., Huyskens, M.H., Lang, X., Xiao, S., Yin, Q.-Z., 2019. Calibrating the terminations of Cryogenian global glaciations. Geology 47 (3), 251–254. https://doi.org/10.1130/G45719.1.

Zhu, Z., Campbell, I.H., Allen, C.M., Brocks, J.J., Chen, B., 2022. The temporal distribution of Earth's supermountains and their potential link to the rise of atmospheric oxygen and biological evolution. Earth Planet. Sci. Lett. 580, 117391. https://doi.org/10.1016/j.epsl.2022.117391.